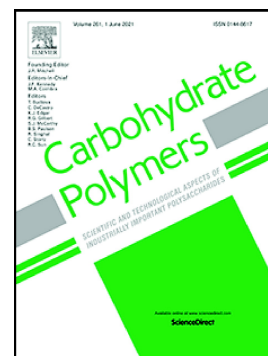


Evaluation of calcium alginate bead formation kinetics: an integrated analysis through light microscopy, rheology and microstructural SAXS

Andrés Posbeyikian, Esteban Tubert, Alejandro Bacigalupe, Mariano Martín Escobar, Patricio Román Santagapita, Gabriela Amodeo, Mercedes Perullini



PII: S0144-8617(21)00680-9

DOI: <https://doi.org/10.1016/j.carbpol.2021.118293>

Reference: CARP 118293

To appear in: *Carbohydrate Polymers*

Received date: 26 February 2021

Revised date: 20 May 2021

Accepted date: 31 May 2021

Please cite this article as: A. Posbeyikian, E. Tubert, A. Bacigalupe, et al., Evaluation of calcium alginate bead formation kinetics: an integrated analysis through light microscopy, rheology and microstructural SAXS, *Carbohydrate Polymers* (2021), <https://doi.org/10.1016/j.carbpol.2021.118293>

This is a PDF file of an article that has undergone enhancements after acceptance, such as the addition of a cover page and metadata, and formatting for readability, but it is not yet the definitive version of record. This version will undergo additional copyediting, typesetting and review before it is published in its final form, but we are providing this version to give early visibility of the article. Please note that, during the production process, errors may be discovered which could affect the content, and all legal disclaimers that apply to the journal pertain.

Evaluation of calcium alginate bead formation kinetics: an integrated analysis through light microscopy, rheology and microstructural SAXS

Andrés Posbeyikian^{a,b,1}, Esteban Tubert^{a,b,1}, Alejandro Bacigalupe^c, Mariano Martin Escobar^c,
Patricio Román Santagapita^{f,g}, Gabriela Amodeo^{a,b,*} amodeo@bg.fcen.uba.ar, Mercedes
Perullini^{d,e,*} mercedesp@qi.fcen.uba.ar

^aDepartamento de Biodiversidad y Biología Experimental, Facultad de Ciencias Exactas y Naturales, Universidad de Buenos Aires, Argentina

^bInstituto de Biodiversidad y Biología Experimental, Universidad de Buenos Aires y Consejo de Investigaciones Científicas y Técnicas, Buenos Aires, Argentina

^cDirección Técnica de Materiales Avanzados, Instituto Nacional de Tecnología Industrial (INTI), Argentina.

^dDepartamento de Química Inorgánica, Analítica y Química Física (DQIAQF), Facultad de Ciencias Exactas y Naturales, Universidad de Buenos Aires, Argentina.

^eInstituto de Química de Materiales medio Ambiente y Energía (INQUIMAE), Universidad de Buenos Aires y Consejo de Investigaciones Científicas y Técnicas, Buenos Aires, Argentina

^fDepartamento de Química Orgánica, Facultad de Ciencias Exactas y Naturales, Universidad de Buenos Aires, Argentina

^gCentro de Investigaciones en Hidratos de Carbono (CIHIDECAR), CONICET-Universidad de Buenos Aires, Argentina

*Corresponding authors.

Abstract

Ca(II)-alginate beads are being produced for a broad spectrum of biotechnological uses. Despite the simplicity of their manufacturing process, in these highly complex arrangements, the final properties of the material strongly depend on the supramolecular scaffolding. Here we present a cost-effective automatized Optical Video Microscopy approach for *in situ* evaluation of the kinetics of alginate bead formation. With simple mathematic modeling of the acquired data, we obtained key parameters that reveal valuable information on the system: the time course of gel-front migration correlates with the plateau of the storage module, and total volume shrinkage is highly related to the stabilization of shear strain and shear stress at the yield point. Our results provide feasible and reproducible tools, which allow for a better interpretation of bead formation kinetics and a rapid

¹ These two authors contributed equally to this work.

screening technique to use while designing gelling materials with specific properties for technological applications.

Key words

Ca(II)-alginate beads; Optical Video Microscopy; gelling front; syneresis; rheological characterization; SAXS microstructure

1. Introduction

Alginic acid (Alg) is a collective term applied to a sustainable and eco-friendly family of exopolysaccharides produced by brown algae and several bacteria. Alg is a linear copolymer formed by residues of (1-4)-linked β -D-mannuronic acid (M) and α -L-guluronic acid (G) in different proportions and sequential arrangements with varying molecular weights (Donati et al., 2005). These biopolymers are widely used among several industries mainly because of their ability to form gels by acid precipitation (acidic gels) or ionic cross linking in the presence of di- or trivalent cations (ionic gels), being Ca^{2+} the most extended cation used, due to low cost, biocompatibility and availability (Grant, Morris, Rees, Smith & Thom, 1973; Draget, Smidsrod & SkjakBraek, 2005; Spedalieri et al., 2015; Sonogo, Santagapita, Perullini & Jobbágy, 2016). By modulating the synthesis formulation parameters, entirely different beads can be produced to satisfy contrasting application requirements (Zazzali Calvo, Ruíz-Henestrosa, Santagapita & Perullini, 2019; Lee, Ravindra & Chan, 2013). Moreover, the possibility of combining alginate with other organic or inorganic systems and the use of additives to finely tune the microstructure of the resulting encapsulation matrix has established alginate as a very versatile material for the immobilization of diverse bio-entities (Calvaia et al., 2016; Florez-Castillo et al., 2019; Perullini, Orias, Durrieu, Jobbágy & Bilmes, 2011). Thus, its biotechnological use has gained a broad spectrum of applications, from cell transplantation to slow release of fertilizers in the agro-industrial sector (Wang, Gao, Zimmerman, Zheng & Lyu, 2018; Anamizu & Tabata, 2019).

The final properties of the material (*i.e.* release rate of a substance, structural hardness, etc.) are highly dependent on the supramolecular chemistry of the beads (Aguirre Calvo, Santagapita & Perullini, 2018). The elucidation of the microstructure-function relationships is consequently of massive importance to industry and research environments in quest of applying a rational design approach to the formulation of alginate-based capsules (Agulhon, Robitzer, David & Quignard, 2012). The standard methodologies used to analyze the supramolecular structure are high-resolution electronic microscopies (SEM, TEM), nuclear magnetic resonance (RMN), and small angle X-ray scattering (SAXS) (Chan et al., 2011; Schuster, Cucheval, Lundin & Williams, 2011).

This last technique is based on correlating the X-ray scattering with the fluctuations in the electron density of the hydrogel lattice in an illuminated sample volume of $\sim 1 \text{ mm}^3$, and allows inferring information about the structure of the native hydrogel on a scale of 1 to 100 nm (Traffano-Schiffo, Castro-Giraldez, Fito, Perullini & Santagapita, 2018). The mechanical behavior of alginate beads – highly dependent on the microstructure of the alginate network- has been evaluated through compression tests^{Error! Bookmark not defined.}, and dynamic or oscillatory tests, revealing information about their viscoelastic properties and providing a rich mathematical framework for evaluating the curing kinetics of these polymer systems (Fu, Thacker, Sperger & Boni, 2011; Gila Vilchez, Bonhome-Espinosa, Kuzhir, Zubarev & Duran, 2018). Rheology is a useful technique to study and understand the kinematics of cross-linking reactions of several polymer-based systems (Bonino et al., 2011; Fernández Ferrés & Norton, 2014). The rheology of the cross-linking reaction of chitosan beads has been studied, measuring the evolution over time of G' , G'' and $\tan \delta$, and has established the “gel time” as the moment in which $\tan \delta$ is equal to 1 (Barreiro-Iglesias et al., 2005). Through these measurements, a relationship has been established between gel time and the cross-linking medium’s concentration. The rheological study of crosslinked fish gelatins has demonstrated that the cross-linking reaction leads to an increase in the G' value (Chiou et al., 2006). Other authors have investigated the rheology of crosslinking guar gum with glutaraldehyde by performing frequency sweep tests at varying temperatures. The authors determined the gel time as the moment when G' and G'' run parallel (Sánchez et al., 2009). The effects of transglutaminase and calcium ions on the structure and rheology of whey protein emulsion gels have also been studied. Rheological properties have been determined by frequency sweep tests and through the study of viscosity curves. In frequency sweep results, an increase in G' has indicated the strengthening of the gel network, while viscosity curves have shown that the increasing shear rates caused the partial destruction of the aggregated protein network structure (Liang et al., 2020). Despite the extended literature on the rheology of curing kinetics of polymer-based hydrogels, we could not find studies of oscillatory rheology of alginate beads and/or capsules.

Currently, $\text{Ca}(\text{II})$ alginate capsules are being produced worldwide at many scales and levels with low-tech equipment due to their unsophisticated synthesis methodology. Being able to follow the bead’s evolution during the synthesis process is clearly of major importance for effective decision-making in regard to the optimization of a specific bead system. A property that allows characterizing the formation process is the reduction in volume due to water expulsion (syneresis), and a simple and economical approach for monitoring a volume changing system is optical video microscopy (OVM). Although previous authors have described the use of optical systems to perform observations on alginate beads, several of those studies only include the evaluation of final shape and size (Hajifathaliha et al., 2020). The aim of this work was therefore to characterize the formation of alginate bead systems using simple, convenient and relatively inexpensive tools to achieve valuable measurements that could replace or complement the more complex traditional

assessments. Our automatized OVM approach allows for *in situ* evaluation of the kinetics of alginate hydrogel formation (gel front migration) along with the kinetics of shrinkage caused by syneresis during alginate bead formation. The experimental design implies a series of technical challenges including the general set-up, lighting arrangement, and automatized image sampling and processing protocols, overcoming one of the limitations in optimizing these approaches: that most alginate beads are completely translucent. We connect the information gathered through OVM with rheological and microstructural analyses and propose a relatively simple model to describe the evolution of this complex system, accounting for the changes produced by the different processes involved by grouping them in short-term and long-term factors. We believe our results would not only be useful to a wide community of scientists and manufacturers who require easy and quick methods for screening different synthesis conditions to evaluate and optimize their formulations, but would also open a framework to unravel kinetic features of the processes involved in alginate bead synthesis.

2. Materials and Methods

2.1 Reagents

Materials employed are listed below: Alginic acid sodium salt (Sigma-Aldrich) molecular weight 120,000-190,000 g.mol⁻¹ and mannuronate/guluronate ratio of 1.56; kaolinite 258,071 g.mol⁻¹ (Imerys, Argentina); methylene blue (MB) (Diopack, Zárate, Buenos Aires, Argentina) molecular weight of 319.86 g.mol⁻¹; anhydrous CaCl₂ (Cicarelli, San Lorenzo, Santa Fe, Argentina) molecular weight of 110.99 g.mol⁻¹. Strontium aluminate 205.58 g.mol⁻¹ (Vortex, Argentina).

2.2 Hydrogel Bead Generation

Alginate beads were prepared by extruding a solution of sodium alginate (dyed, when indicated) as droplets, into a divalent cross-linking solution of CaCl₂ at 0.1 M concentration. In general, beads greater than 1.0 mm in diameter can be prepared by using a syringe with a needle or a pipette (Gombotz, 1998). In this work we employed a 200 µL micropipette (Gilson P200). Details on each alginate system prepared as well as the image sampling protocol and the image processing are presented in Supplementary Information.

2.3 Small Angle X-Ray Spectroscopy

The structure of the Ca(II)-alginate matrices with or without the addition of contrasting agents has been modeled as a mass fractal system of interconnected alginate rods, as previously reported (Agulhon et al., 2012). This microstructure was characterized by small angle X-ray scattering (SAXS) as initially described by Agulhon and co-workers (2012) with the modifications included by Traffano-Schiffo and co-workers (2018) for Ca(II)-alginate matrices with different additives. According to this model, from the slope of the SAXS curve ($I(q)$ in logarithmic scale vs. q , as shown in Fig. 8), three parameters can be derived: the fractal dimension at low q (α_1) describing the degree of interconnection of the alginate rods composing the structure, the fractal dimension at intermediate values of q (α_2) describing the degree of compactness within the rods, and the fractal dimension at high values of q (α_3) related to the connectivity between associated polymer chains forming dimers. Additionally, the characteristic radius of rods (R_1) and the radius of the alginate dimers (R_2), can be derived from the points of change in fractal regime (*i. e.* in the slope of the SAXS profiles). SAXS measurements were performed at the LCLS SAXS1 beam line in Campinas, Brazil, working at $\lambda = 0.1488$ nm and wave vector was selected in the range $0.142 \text{ nm}^{-1} < q < 5.035 \text{ nm}^{-1}$.

2.4 Oscillatory Rheology

Rheological characterizations were made in an oscillatory rheometer (MCR301, Anton Paar, Austria) equipped with a 25 mm diameter steel plate geometry. Tests were carried out in a controlled shear strain range from 0.001 to 100% at a constant shear frequency of 10 s^{-1} . All the rheological measurements were tested at a constant temperature of 25°C and a relative humidity of 50%. Drops of 2 % sodium alginate solution were submerged in the 0.1 M CaCl_2 solution in a time range from 5 to 21600 s. The beads were washed with distilled water and dried prior to placing them between the rheometer plates. Beads were carefully placed on the plate in order to reduce to a minimum the gap between samples. The sodium alginate solution was also measured to obtain the values at $t = 0$ s (before gelation).

3. Results and Discussion

3.1 Design of a video microscopy set-up to study the bead formation kinetics

To analyse the formation kinetics of the alginate beads *in situ*, we adapted a proven methodology previously reported for measurement of volume changes against time in *Xenopus laevis* oocytes that overexpress aquaporins after a shift in the medium's osmolarity (Ozu, Alvarez,

Mccarthy, Grigera & Chara, 2013; Ozu, Galizia, Acuña & Amodeo, 2018). Schematically, this adapted method consists in using a vibration-stabilized stereoscopic microscope with a mounted digital camera and a specially designed chamber that holds the cross-linking medium, which ensures that a single bead can be easily positioned at the microscope's optical target, allowing images to be taken with an undisturbed focus (Figure 1A and C).

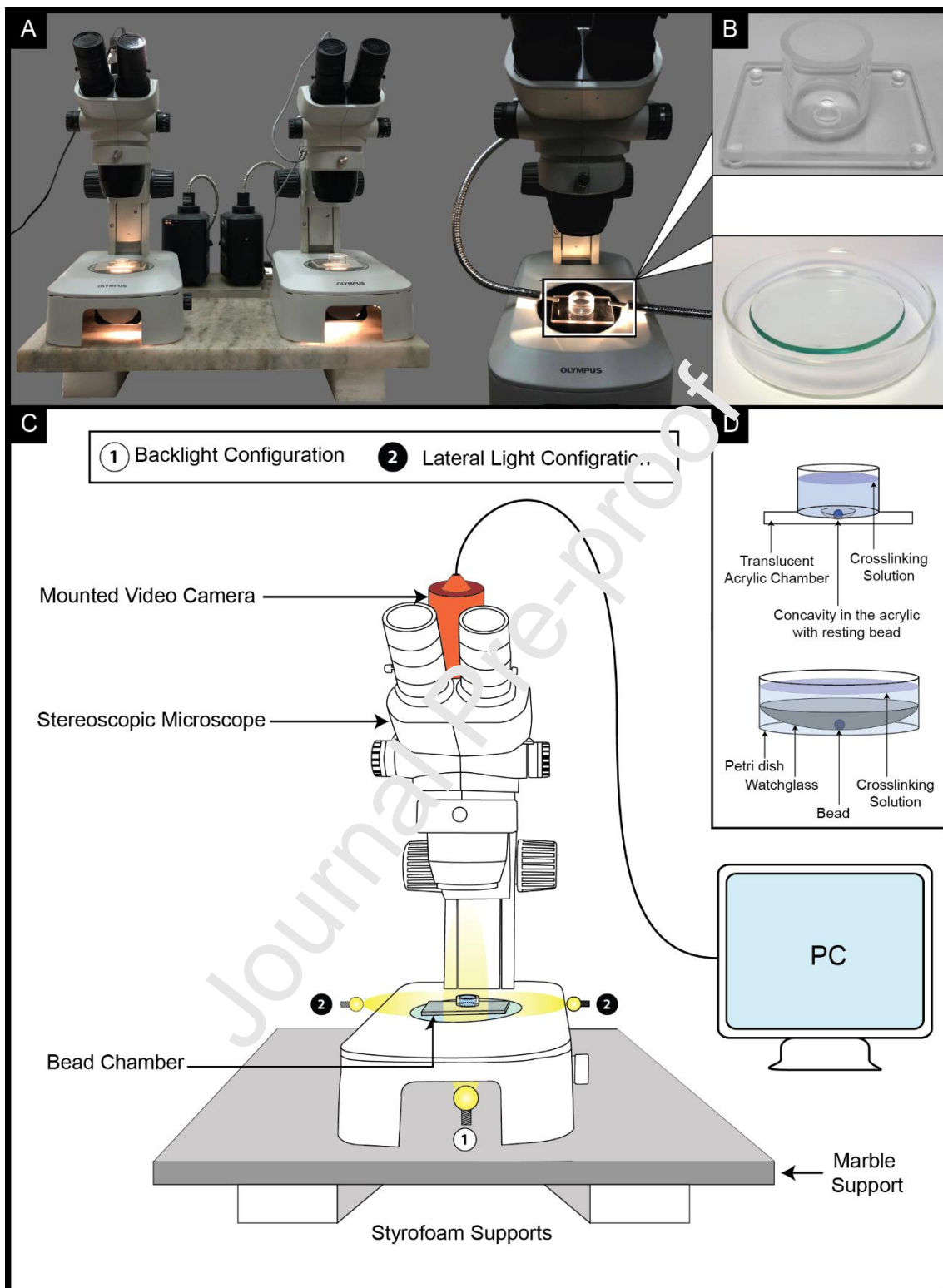


Figure 1: A) Pictures of the microscopy set-up used to measure bead volume change over time; to the left, two stereo microscopes in the backlit configuration, to the right, a laterally lit chamber. **B)** Detailed images of the two types of chambers that can be employed, with two proposed options, one made from carved acrylic, the other from glass. **C, D)** Illustrated and labeled diagrams describing the set-up.

The system also relies upon software automatization to regulate the sampling rate while taking successive images during the bead synthesis. Each individual image obtained from a given time-course is filtered for circularity, passed through a threshold filter and converted to a binary image. If the beads are considered spherical, the sampled picture can be measured to obtain the area of a bead's great circle (orthodrome) at a given time. Further processing of these measurements can yield the instantaneous volume of the bead for each moment in time during the gelation process, which in turn can be converted to variables of interest such as volume or water flux (Sutka, Amodeo & Ozu, 2017). In this work, the medium used was a cross-linking solution (0.1 M CaCl_2) into which a single alginate solution drop was released. Considering the extensive length of the syneresis experiments (up to 6 hours of duration), a major concern is the stabilization of the bead. In view of this, to hold the cross-linking medium and the bead steady, we designed and evaluated two alternative chambers. The preferred system (Chamber A) consisted of a transparent acrylic support plate -which presents a central concavity- stuck to a cylindrical piece, which together formed a 10 ml blunt chamber. The presence of the central concavity allowed for the bead to easily remain centered after being released, yielding good quality and stable measurements that could be properly processed and converted into the variables of interest (Figure 1-B and 1-D). An alternative simpler system, which consisted of a glass Petri dish holding a watch glass (Chamber B) was also analyzed, yielding good results as well (Figure 1B and D). Similarly, the watch glass (being cheaper and readily available in the market) allows the bead to fall into a centered position, remaining fixed in place during the measurements.

Two types of experiments were conducted: *syneresis kinetics* assays (measuring volume change of beads during a 6-hour period after the introduction of the alginate drop into the cross-linking solution) and *gelling front evolution* assays (a process which takes approximately 10-15 minutes for the systems under study). One of the major drawbacks of evaluating the syneresis kinetics of alginate beads using light microscopy is their translucency, which makes capturing good quality images a challenging task (Figure 2). Although certain lighting configurations allowed for the measurement of the bead's area by hand (manually fitting an ellipse over the region of interest) no lighting configuration yielded the high contrast images needed for correct automatic image analysis. In view of this, the introduction of a reflecting opacifier to the alginate solution was explored, to

achieve proper contrast. The opacifier: i.) should be retained within the alginate bead during the time-course of the experiment, ii.) should not significantly modify the microstructural properties of the system and should not interfere with the gelation process, iii.) must reflect light sufficiently, iv.) must spread evenly in the matrix, and v.) should ideally be an available and inexpensive material. We first opted for a phosphorescent powder dye (strontium silicate-aluminate) with the objective of producing the highest possible contrast against a dark background. Although excellent contrast was achieved, it was only at high concentrations of the phosphorescent dye (in relation to alginate mass), altering the alginate network microstructure, as will be further discussed. At lower concentrations, the distribution of the dye particles was uneven, possibly due to the larger-than-desired particle size (Supplementary Figure SI-1). Since the concentration of the opacifier should be the lowest possible to prevent interactions with the alginate chains and/or with the active substances loaded within the beads, the search was directed toward insoluble nano-particulate materials, capable of producing a darkening effect in water based solutions by forming stable colloidal suspensions. This led us to a group of materials known as nano-clays, which are natural clay minerals that have the advantage of presenting nanometric sized particles with fairly homogeneous size distributions. Bentonite and kaolinite appeared to be acceptable candidates, since they have already been formulated into alginate bead systems with other purposes (da Silva Fernandes, de Moura, Glenn & Aouada, 2010). Kaolinite was selected, which is a silicate mineral insoluble in water that is generally free of divalent cationic impurities and is easily available at a low cost worldwide (Hartati et al., 2020). Decreasing concentrations of this clay (from 0.20% to 0.02% w/v) were evaluated in alginate bead systems, and it was confirmed that it effectively produces the desired opacifying effect with a lowest viable concentration of only 1:100 with respect to alginate (0.02% w/v), (Figure 2).

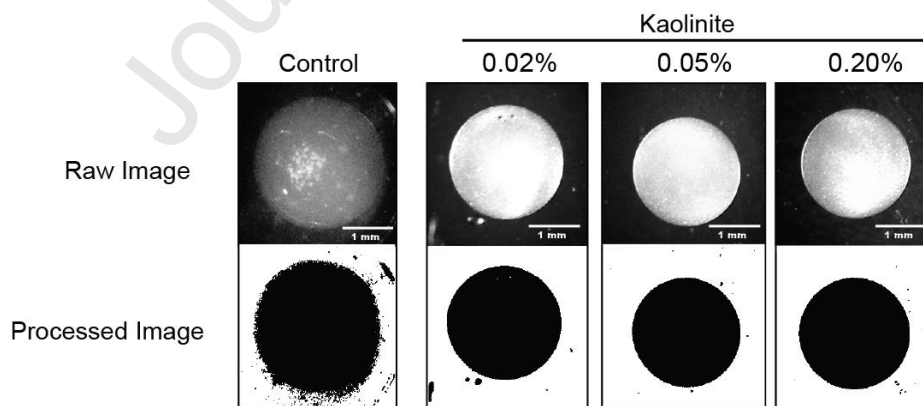


Figure 2: Results obtained using different concentrations of kaolinite as a contrasting agent (0.02, 0.05 and 0.20% w/v). The raw images were processed through the automatic method.

To validate the results obtained through the automatic analysis of the images, they were compared against results obtained through a manual method (manual fitting of an ellipse by four different operators on the images of the synthesis of the beads, at time points evenly distributed on a logarithmic scale of the syneresis process). For this task, images of the 2% alginate-0.05% kaolinite system (Alg2-K) exposed to the cross-linking solution were recorded over 6 hours using the already described set-up. Measurements using kaolinite-free 2% alginate beads (Alg2-C) were performed to control any observable interference that the opacifier could be producing on the syneresis kinetics (Supplementary Figure SI-2). This last system was measured only by means of the manual method, due to its translucency, which made automatic measurements impossible. A dimensionless variable was used to directly compare independent systems: V/V_0 , estimated volume at the evaluated time over the initial estimated volume of the bead. In any given experiment, the first few seconds of the assay yield blurry images as a bead takes around 90 seconds to settle at the bottom of the chamber. Thus, the initial time was defined as the minimum elapsed time since initiation of cross-linking, for which all replicas of all conditions provided a focused image of the bead and in consequence all subsequent bead volumes were normalized by the volume of a given replica at that time (initial time, t_0). The comparison between automatic and manual measurements for the same dataset showed that the latter gives a noisier trend, with higher variability compared to the former ($SD_{\text{Automatic}} = 0.0005$; $SD_{\text{Manual}} = 0.001$). A likely explanation for this observation is that the manual approach estimates the volume of the bead by measuring its area using the software's oval tool, which is subjected to the variability inherent to the human handling of the task (Figure 3A). Contrary to this, the automatic method uses a standardized protocol that sets a threshold for the binarization of all the frames in an experiment, so they are all processed equally, reducing the noise along the curve. Furthermore, the automatic processing of the images from one experiment (with 4 replicas) took approximately 5', while the manual analysis took between 15'-30' for each determination (operator dependent). This means that the automation of the image processing yielded results that were obtained 300-600% faster. Moreover, while the manual method was restricted to analyzing only 20 time points per replica, the automatic method is fast enough to manage measuring 150 images per replica. In sum, the automatic method is not only faster, but it can also provide a higher temporal definition for the representation of the syneresis kinetics curve.

We later employed the validated automatic processing method to make measurements and compare alginate systems at two concentrations, which are expected to behave differently with respect to their volume change against time after initiation of cross-linking. Figure 4 shows the experimental values obtained for samples Alg2-K and Alg3-K along with a fit to a double exponential decay, which is indicative of two-time scale processes occurring in the evolution of these systems in agreement with literature (see the mathematical modeling in Supplementary Information).

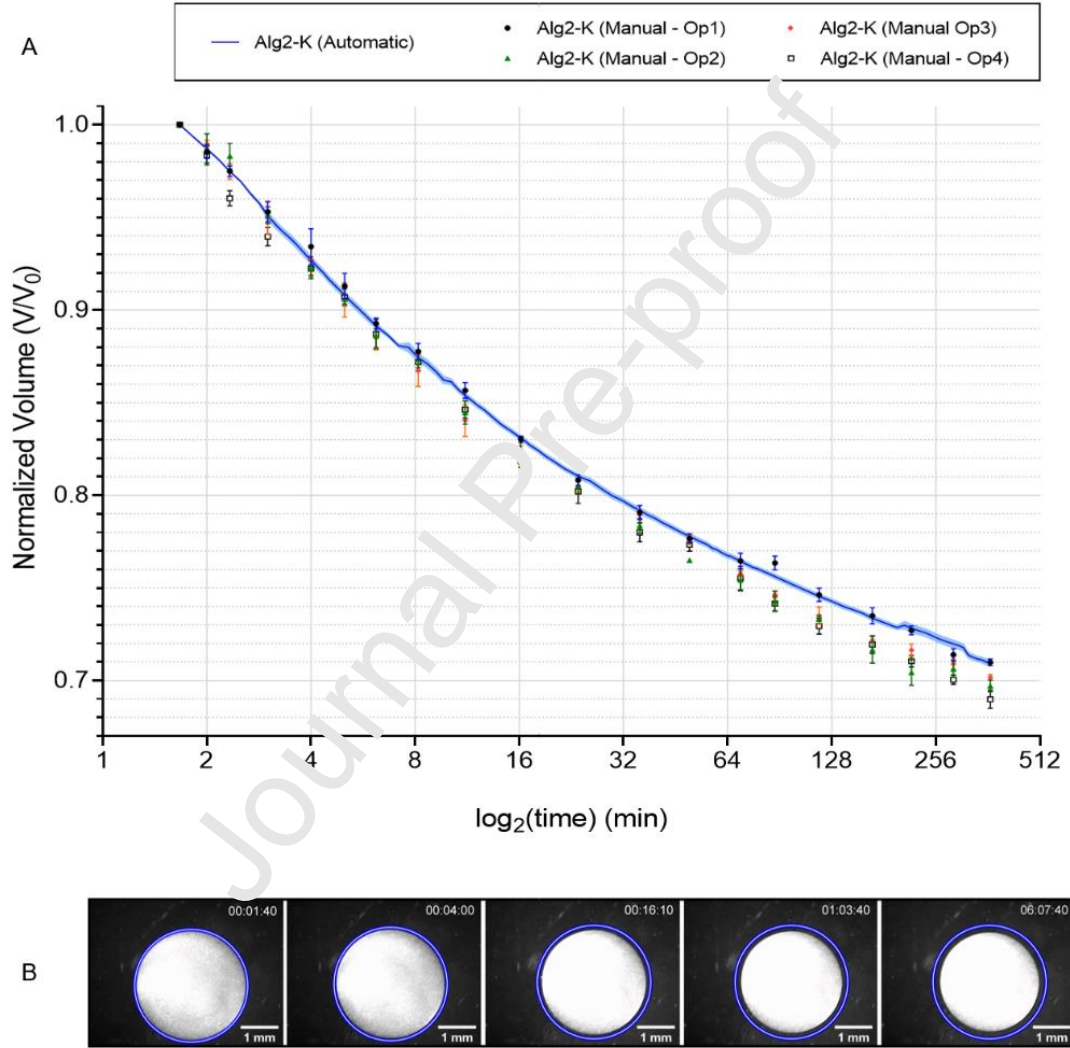


Figure 3: A) The kinetics of the volume change of the 2% alginate, 0.05% kaolinite system (Alg2-K) was recorded over 6 hours using the previously described video microscopy set-up. The obtained images were processed through both an automatic and manual method. The shaded area in the Alg2-K (Automatic) curve corresponds to the Standard Error of the Mean (SEM) ($n = 4$). Four different operators manually recorded bead area at different time intervals of 4 independent experiments (error bars correspond to SEM, $n = 4$). **B)** Raw images at different time points for the Alg2-K system are presented. The bead's initial area was marked in blue as a reference.

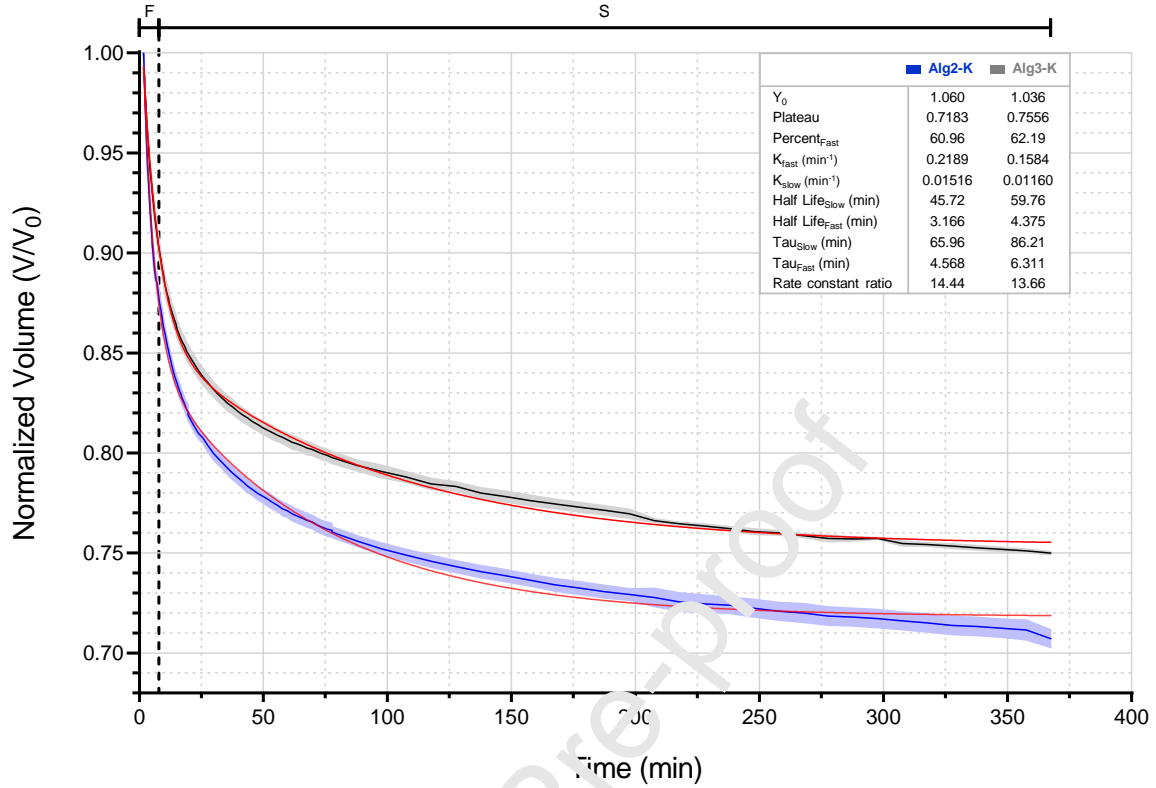


Figure 4: Volume change kinetics followed through video microscopy of 2% and 3% alginate both with addition of 0.05% kaolinite (systems Alg2-K and Alg3-K, respectively). Shaded area corresponds to S.D., $n = 4$. Dotted line at 7 minutes separates the fast process (gelling-front migration) (F) from the slower process (long-term syneresis) (S). Red curves correspond to double exponential decay fits for samples Alg2-K and Alg3-K ($R^2 = 0.9922$ and 0.9917 respectively), with fitted parameters presented in inset.

3.2 Characterization of the gelling front migration

The video microscopy set-up we proposed could also detect other valuable features of the alginate bead synthesis such as the movement of the gelling front, which occurs at the interface of the non-reacted polymer solution and the already cross-linked alginate. This renders a precise line that defines an outer area 'A' (Ca(II)-alginate hydrogel) and an inner area 'a', formed by alginate polymer in solution. These zones appear distinct because of a difference in their refraction index. Therefore, instead of using highly reflective particles (e.g. kaolinite) for dyeing the beads, we used a soluble dye (methylene blue, MB) which allowed a better visualization of the boundary line compared to the other dyeing agents tested. Furthermore, we rearranged the lighting scheme to optimize the detection of the gelling front migration, opting for the laterally-lit configuration rather than the backlit one previously used (Figure 1A and C).

Using this approach, we recorded the evolution of the gelling front in alginate bead systems of 2% and 3% with MB (Alg2-MB and Alg3-MB) and designed an algorithm for tracking the positions of the outer edge of the bead and the gelling-front over time (Figure 5.A-B). The processing reduces

image noise and passes a threshold that creates a binary picture, which allows the Hough Circle Transform algorithm to detect the bead's location very easily. A centroid and a radius are estimated and are used to create an aligned stack of all the recorded images. Radial profiles are then calculated for each time point (Figure 5.C), which are then analyzed to locate peaks, corresponding to maximums in intensity at positions r and r_0 . The inner radius (r : radius of the circle determined by the area a) over the outer radius (r_0 : radius of the circle determined by the area A) can be used as a dimensionless variable to study the advance of the gelling front as a function of the time spanned (Figure 5.D). Completion of gelation (*i.e.* when r/r_0 reaches values below 0.2 and the gelled volume is higher than 99%) was achieved at ca. 330s for Alg2-MB and ca. 440s for Alg3-MB system. To validate the results obtained from the automatic processing of the images, we measured the inner (A) and outer (a) areas manually at 20 time points for both systems, which resulted in similar results (Figure 5.E).

A linear fit of the experimental data obtained through the automatic method is observed in the range r/r_0 0.15 to 0.85. The theoretical justification for this adjustment is presented in Supplementary Information (Supplementary Figure SI-4). For a quantitative comparison between the automatic and manual method, data from each technique was modelled through a linear regression, and the fitted parameters were compared. Results show that the estimation of the rate of movement of the gelling front ($d(r/r_0) / dt$) is similar for both methods, and the standard error is an order of magnitude lower for the automatic method in comparison to the manual method (Table I).

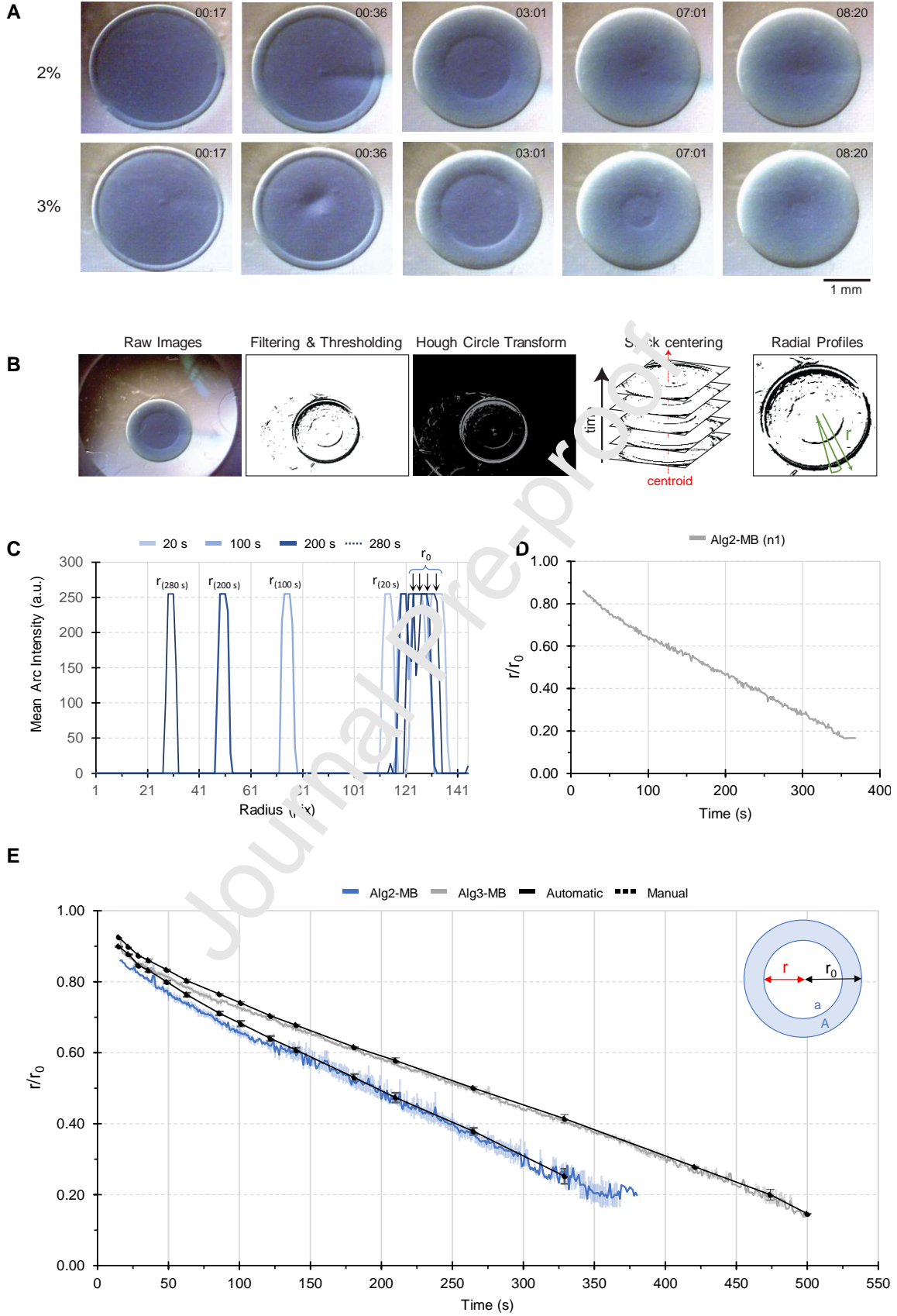


Figure 5: A) Images showing the advance of the gelling front for 2% and 3% alginate, both with 0.01 % w/v methylene blue (Alg2-MB and Alg3-MB, respectively) at different time points during the gelation process (17, 36, 122, 181 and 265 seconds). **B)** Image processing workflow is shown with partial results from each step, using Alg2-MB at 140 seconds of cross-linking. First raw images are filtered for noise and a threshold is applied, next the Hough Circle Transform algorithm finds the bead and returns a radius and a centroid, which are used to align all the slices in the stack. Finally, a radial profile is calculated for each slice, resulting in **C)** Mean Arc Intensity vs. Radius graphs. The radial profiles of 4 different times are shown: 20, 100, 200 and 250 seconds. Peaks corresponding to r (gelling front position) are labeled, as well as those corresponding to r_0 (the bead's outer edge). **D)** The dynamic of r/r_0 is shown for one assay of the Alg2-MB system. The positions of r and r_0 were obtained for each time from the radial profiles shown in (C). **E)** Evolution of the gelling front measured as the dimensionless variable r/r_0 vs. time. Error bars and shading correspond to standard deviation ($n=3$). Both systems show a linear relationship with time for an extended range of r/r_0 . **inset:** diagram showing the two radii involved in the r/r_0 variable. Additionally, in dotted lines, manual measurements at 20 time points were included to validate the automatic method.

	Alg2-MB		Alg3-MB	
	Manual	Automatic	Manual	Automatic
M	$(-1.98 \pm 0.03) \text{ E-3 s}^{-1}$	$(-1.840 \pm 0.009) \text{ E-3 s}^{-1}$	$(-1.503 \pm 0.017) \text{ E-3 s}^{-1}$	$(-1.435 \pm 0.002) \text{ E-3 s}^{-1}$
B	0.894 ± 0.005	0.855 ± 0.002	0.901 ± 0.004	0.8743 ± 0.0007

Table 1: Linear regression parameters estimated for Alg2-MB and Alg3-MB gelling front kinetics assays through automatic and manual methods (m : slope, and b : y-intercept). Mean \pm Standard Error (SE) for the parameters are reported ($n = 2-3$).

3.3 Rheological analysis of the kinetics of alginate beads formation

As previously stated, the formulation variables of alginate beads have an enormous impact on the evolution of their microstructure and, consequently, on the properties of the final systems (Zazzali et al., 2019). Such evolution can be analyzed by measuring viscoelastic properties of the alginate beads against time after cross-linking initiation using an oscillatory rheometer. These measurements complement the data previously gathered through OVM experiments, as well as the microstructural analysis by SAXS. A controlled deformation test was performed on alginate bead samples that were cross-linked during different times (5s to 21600s). After the respective cross-linking times, beads were washed and directly transferred to the rheometer's measuring plate, carefully arranging enough beads (~ 30 units) so that the whole available area was covered. For the first analysis, the storage modulus (G') value was considered in the linear viscoelastic region (LVR) from amplitude sweep tests. The raw data of the rheological measurements are presented in the Supplementary Information (Supplementary Figure SI-3). Results show an increase in the plateau of G' , which represents cohesive strength as a function of the reaction time. Naturally this is related to increased cross-linking among alginate chains, which give greater structural strength to the beads. The initial measurement was done at $t = 5$ s. The evolution of G' was divided into three phases, according to the curve's slope. The first one corresponds to the interval from $t=5$ s to $t=46$ s, the second one ranges from 46s to 1080s (where the maximum value of G' was achieved) and a third one corresponds to data points beyond 1080s, where G' values were constant (Figure 6). It is

worth noting that for this system, $t=46s$ corresponds to the time point at which approximately half of the total initial volume of the drop has gelled (*i.e.* $r/r_0=0.794$; $t=47.3s$) and 1080s corresponds to 3-4 gelation times, considering total gelation as the point at which 99.2% of the volume is gelled (*i.e.* $r/r_0=0.2$; $t=330s$). Beyond this point, minimal changes occur in the structure of the beads (Figure 6) as previously observed in these systems (Larsen et al., 2015). Thus, from the results a dependence can be observed between the bead's viscoelastic coefficient G' Plateau (which refers to the structural strength of each bead) and the previously observed gelling front migration status (measured as the fraction of gelled volume).

The identification of the LVR of the different hydrogels submitted to deformation amplitude sweep tests provides structural information of the systems (Buffle, Zhang & Startchev, 2007). Figure 7 shows the shear strain at the yield point as a function of the cross-linking duration. Three phases can be clearly defined: an initial phase where the yield point occurs at high shear strain values ($\sim 100\%$), exhibiting a great capacity for recovery. At this stage ($t < 15s$), the system is a liquid volume surrounded by a thin layer of Ca(II)-alginate hydrogel; the concentrations of non-crosslinked Alg polymer and Ca^{2+} cations are high, and thus the possibility of rearrangement of the structure is significant. A second stage extends from approximately $t=15s$ to $t=300s$ (in coincidence with the linear regime observed for the evolution of the gelling front in Figure 5), the recovery capacity of the structure decreases as the layer of hydrogel progressively thickens. In a third stage, approximately from $t > 300s$, shear strain remains constant ($< 0.6\%$), meaning that no significant structural change can be reached after almost the total volume of the bead is gelled.

An increment in G' , which corresponds to the elastic portion of G modulus obtained from Hooke's law, means that the beads become stiffer as the reaction proceeds. On the other hand, the yield point represents the linearity limit of G' . Beyond this limit, the internal structure begins to break due to the applied strain. According to the results shown in Figures 6 and 7, the progress of the cross-linking reaction generates stiffer and more brittle beads that deform irreversibly at lower shear strain values. The increasing amount of new chemical interactions produces more rigid hydrogels, while physical interactions give rise to soft and flexible systems (Gila-Vilchez et al., 2018). The rheological parameters here analyzed provide significant information about the gelling status of the hydrogel beads, and therefore allow a more complete understanding of bead formation kinetics.

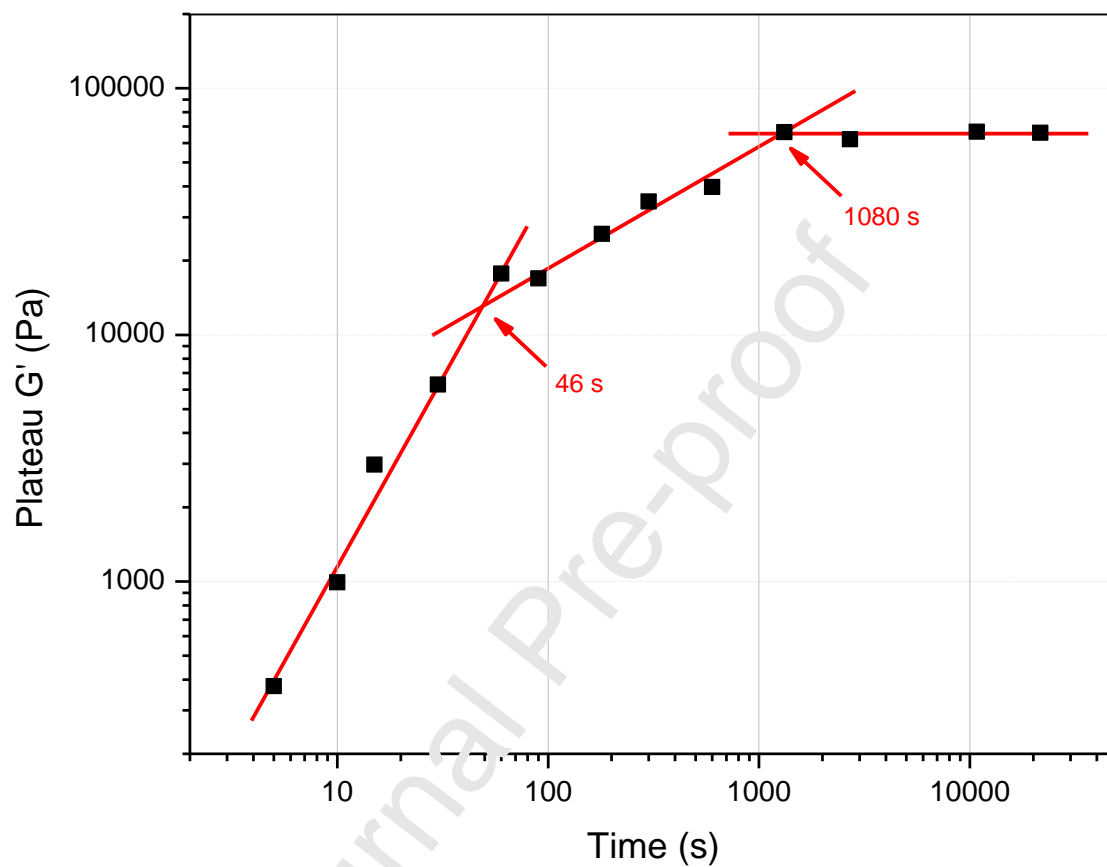


Figure 6: The plateau of G' as a function of time. Different regions are observed: abrupt increase in G' for $t < 46$ s, slight increase in G' for intermediate times, and constant maximum value of G' for $t > 1080$ s.

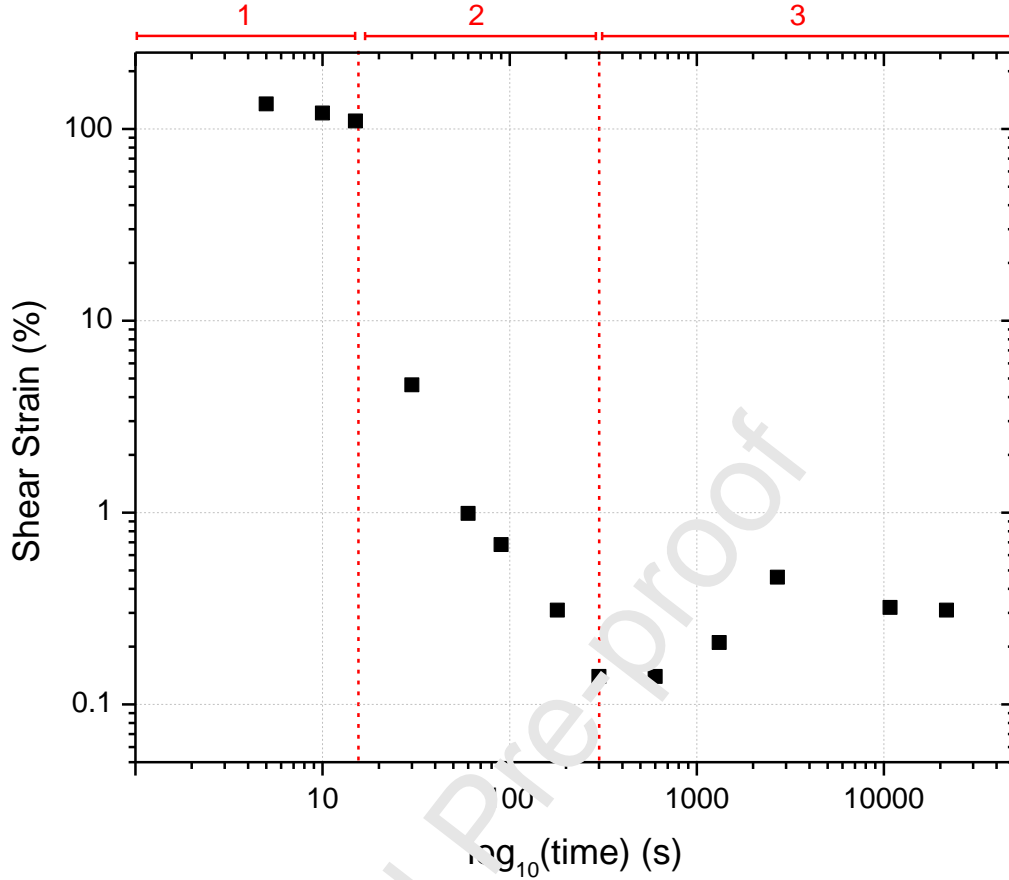


Figure 7: Shear strain values at the view point as a dependence of time (logarithmic scale).

3.4 Microstructural analysis

The capacity to precisely measure the evolution of Ca(II)-Alg systems by means of the OVM set-up involves the inclusion of dyes or scattering microparticles (marking agents) within the polymer matrix. In Figure 8 we present the microstructural parameters derived from the analysis of Small Angle X-ray Scattering curves, evaluating the impact of the different marking agents employed: 0.05 % kaolinite (K), 2.5% strontium aluminate fluorophore (FF), and 0.01 % methylene blue dye (MB).

As for previous studies, Ca(II)-alginate hydrogels showed isotropic scattering and were modeled as a fractal system composed of rods (Liu, Li, H., Tang, Bi, Li, L., 2016; Traffano-Schiffo et al., 2018). The gelation occurs through a so called sol-gel process: precursors (alginate chains and Ca^{2+} cations) originally in solution interact to form dimers, characterized by their size (parameter R_2) and density (parameter α_3), which in turn form rod-like structures composed of several dimers,

characterized by their size and compactness (R_1 and α_2 , respectively) that interconnect to form a ramified network (parameter α_1 is related to its degree of ramification).

At the smallest scale, parameter α_3 does not present significant differences among samples, showing a typical value (a fractal density ~ 1 at the scale of dimers indicates long dimer chains, with almost no ramifications or perturbations). This result is indicative of an ordered dimer formation for all systems. However, analyzing the parameter R_2 , related to the size of these basic units, slight differences can be observed. In general terms, a higher concentration of precursors (Alg polymer and Ca^{2+}) is expected to generate a higher concentration of nucleation sites (dimers formation). However, the relative availability of Ca^{2+} will depend on the ratio $[\text{Ca}^{2+}]/[\text{G-block sites}]$, which is higher for 2% Alg samples. Thus, with increasing availability of Ca^{2+} during the formation of dimers there is a reduced possibility of rearrangement and densification of the dimer structure (*i.e.* higher values of parameter R_2). The modulation of parameter R_2 caused by the addition of marking agents is even smaller, showing a tendency to increase the size of dimers, probably by causing a perturbation in the dimerization process but without intercalating in Alg dimers. It is worth noting that for 2% Alg samples only the addition of the FF caused a significant increase in R_2 .

When analyzing the modulation of the microstructure at the rod-scale, in 3% Alg samples (high Alg concentration), events of nucleation of dimers forming rods are more frequent, generating a higher concentration of rods that result smaller in size (lower R_1). Regarding the fractal dimension within the rods (α_2), it is attributable to the degree of order in which dimers nucleate and aggregate during the formation of these structures, and the relative concentration of Ca^{2+} has an important effect in the kinetics of the process. At a relative high concentration of Ca^{2+} (Alg 2% samples), the reordering of polymer branches to maximize weak interactions is hindered by a rapid cross-linking of the initial structure by Ca^{2+} . As predicted from this, in Figure 8, the values of parameter α_2 increase for 2% Alg samples. Once again, the effect of the marking agents on the size of the rods is minimal, showing no significant difference for 3% Alg formulations, and only a slight decrease for samples FF and K in the 2% Alg samples. This last effect could be attributable to the impeded diffusion of Alg branches caused by a particulate marking agent.

At a larger scale, the fractal dimension of the rods network (α_1) will depend on the facility of the rods to interconnect. For a lower Alg concentration (2% samples), the kinetics of nucleation and aggregation of dimers is relatively slow, and the forming unsaturated rods (*i.e.* with free branches of non-linked polymer) are more likely to interconnect forming a 3D network (higher values of parameter α_1). When comparing within the different systems studied here, the presence of a marking agent generates a more branched structure (higher α_1 in K, FF and MB systems compared to their correspondent control, regardless of the Alg concentration). This could result from a direct perturbation during the first steps of the sol-gel process (*i.e.* even before the percolation of the system), forcing the growing rods to branch more frequently.

The use of kaolinite as an additive for synthesis in order to improve the visualization of the Ca(II)-Alg beads, produces a minimum perturbation of the system at the microstructural level. Only certain microstructural parameters present slight differences with respect to the control systems, for both set of samples analyzed (2% and 3% Alg). It is important to note that these differences in microstructural parameters observed are similar to those caused by the addition of 0.01% w/v MB dye (*i.e.* a relatively small molecule $MW = 319.8 \text{ g.mol}^{-1}$), which is not expected to interfere with the calcium alginate sol-gel process. Finally, the use of strontium aluminate, although being a good marker agent for the video microscopy technique, resulted not appropriate in view of the changes that causes in the system at the microstructural level (specially the increase in α_1 from 1.33 to 1.61, and the increase in α_2 from 2.4 to 3.0).

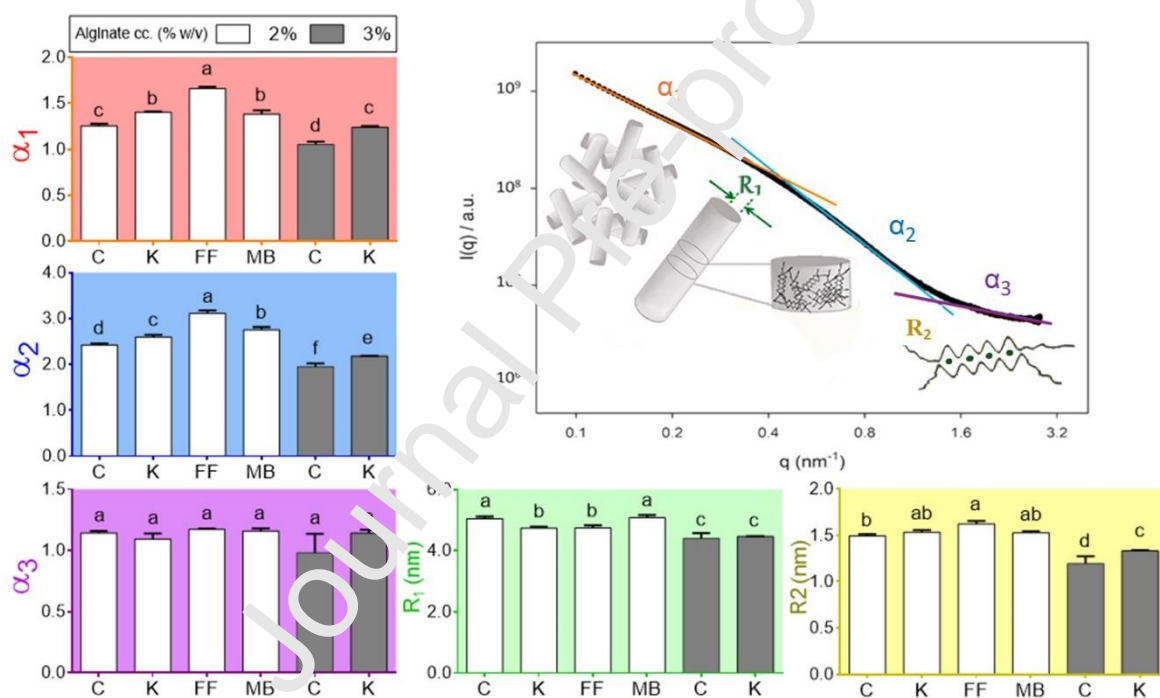


Figure 8: Microstructural parameters obtained from SAXS experiments conducted on the 2 and 3% alginate systems, dyed with different substances. 2% alginate beads (white bars): control sample (C), sample with 0.05% w/v kaolinite (K), with 2.5% w/v strontium aluminate (FF), and with 0.01% w/v methylene blue (MB); 3% alginate beads (grey bars): control sample (C) and sample with 0.05% w/v kaolinite (K). The $I(q)$ vs q curves obtained were each fitted to obtain three parameters related to the fractal density of the alginate matrix at different scales (α_1 , α_2 and α_3) and parameters R_1 and R_2 , which give information about the diameter of the alginate rods, and the distance between alginate chains in dimers, respectively. Error bars correspond to standard deviation ($n \geq 3$).

3.5 Modeling of experimental results

A detailed modeling of the experimental results to account for both the first stages of the bead formation and the evolution of the beads on a long-term basis is presented in Supplementary Information.

4. Conclusions

The Ca(II)-alginate bead formation relies on several different processes and its kinetics are dependent on many synthesis parameters (e.g. alginate and cross-linking solution's concentration, or cation nature). Its detailed modeling is not only complex and time-consuming, but more importantly it makes assumptions that are valid only in a restricted range of conditions. Thus, for the optimization of certain applications it results impracticable. Here we demonstrate that the mechanical behavior of the studied system is highly related to the evolution of the gelling front and the total volume of the beads, which can be obtained by means of the extremely simple Optical Video Microscopy (OVM) characterization tool presented here, without the need for sophisticated equipment.

The addition of specific contracting dyes allows for automatic processing of image data, highly improving the efficiency of the proposed characterization tool, without significantly altering the microstructural parameters of the alginate network. Moreover, the phenomenological fitting of the experimental results proposed for the analysis of the data obtained, shows that this powerful characterization method is versatile, practical and easy to implement for the optimization of Ca(II)-alginate systems designed for scientific or technological approaches.

Acknowledgments

This work was supported by the Brazilian Synchrotron Light Laboratory (LNLS, Brazil, proposal SAXS1-20190143 and SAXS1-20190073), Agencia Nacional de Promoción Científica y Tecnológica (ANPCyT PICT-2017-0569 and ANPCyT PICT-16 2365) and University of Buenos Aires (UBACyT18-20).

Supplementary data

Supplementary material

References

- Abang, S., Chan E-S., Poncelet, D. 2012, Effects of process variables on the encapsulation of oil in Ca-alginate capsules using an inverse gelation technique, *Journal of Microencapsulation*; 29(5): 417–428.
- Aguirre Calvo, T. R., Perullini, M., Santagapita, P. R. 2018, Encapsulation of betacyanins and polyphenols extracted from leaves and stems of beetroot in Ca(II)-alginate beads: A structural study, *Journal of Food Engineering*, 235, 32-40.
- Agulhon, P., Robitzer, M., David, L., & Quignard, F. 2012, Structural regime identification in ionotropic alginate gels: Influence of the cation nature and alginate structure, *Biomacromolecules*, 13(1), 215–220.
- Anamizu, M., Tabata, Y. 2019, Design of injectable hydrogels of gelatin and alginate with ferric ions for cell transplantation, *Acta Biomaterialia*, 100, 184-190.
- Barreiro-Iglesias, R., Coronilla, R., Concheiro, A., & Alvarez-Lorenzo, C. (2005). Preparation of chitosan beads by simultaneous cross-linking/ insolubilisation in basic pH: Rheological optimisation and drug loading/release behaviour. *European Journal of Pharmaceutical Sciences*, 24(1), 77–84. <https://doi.org/10.1016/j.ejps.2004.09.013>
- Bonino, C. A., Samorezov, J. E., Jeon, O., Alsberg, E., & Khan, S. A. (2011). Real-time in situ rheology of alginate hydrogel photocrosslinking. *Soft Matter*, 7(24), 11510–11517. <https://doi.org/10.1039/c1sm06109g>
- Buffle, J., Zhang, Z., Startchev, K. 2007, Metal Flux and Dynamic Speciation at (Bio)interfaces. Part I: Critical Evaluation and Compilation of Physicochemical Parameters for Complexes with Simple Ligands and Fulvic/Humic Substances. *Environmental Science and Technology*, 41, 22, 7609–7620.
- Carbajal, M., Perullini, M., Jobbány, M., Ullrich, R., Hofrichter, M., Levin, L. 2016, Removal of phenol by immobilization of *Trametes versicolor* in silica-alginate-fungus biocomposites and loofa sponge. Contribution of ligninolytic enzymes to the process, *Clean-Soil and Water*, 44 (2), 180-188.
- Chan, E-S., Lim, T-K., Voo, W-P., Pogaku, R., Tey, B. T., Zhang, Z. 2011, Effect of formulation of alginate beads on their mechanical behavior and stiffness, *Particuology*, 9 (3), 228-234
- Chiou, B. Sen, Avena-Bustillos, R. J., Shey, J., Yee, E., Bechtel, P. J., Imam, S. H., Glenn, G. M., & Orts, W. J. (2006). Rheological and mechanical properties of cross-linked fish gelatins. *Polymer*, 47(18), 6379–6386. <https://doi.org/10.1016/j.polymer.2006.07.004>
- da Silva Fernandes, R., de Moura, M. R., Glenn, G. M., Aouada, F. A. 2018, Thermal, microstructural, and spectroscopic analysis of Ca²⁺alginate/clay nanocomposite hydrogel beads, *Journal of Molecular Liquids*, 265, 327-336.
- Donati, I., Holtan, S., Morch, Y. A., Borgogna, M., Dentini, M., Skjak-Braek, G. 2005, New hypothesis on the role of alternating sequences in calcium-alginate gels, *Biomacromolecules*, 6, 1031-1040.
- Draget, K. I., Smidsrod, O., SkjakBraek, G. *Polysaccharides and Polyamides in the Food Industry. Properties, Production, and Patents.*; Steinbuchel, A., Rhee, S. K., Eds.; Wiley-VCH Verlag GmbH & Co. KGaA: Weinheim, 2005; p 1.

- Fernández Farrés, I., & Norton, I. T. (2014). Formation kinetics and rheology of alginate fluid gels produced by in-situ calcium release. *Food Hydrocolloids*, 40, 76–84. <https://doi.org/10.1016/j.foodhyd.2014.02.005>
- Flórez-Castillo, JM, Ropero-Vega, JL, Perullini, M Jobbágy. M. 2019, Biopolymeric pellets of polyvinyl alcohol and alginate for the encapsulation of Ib-M6 peptide and its antimicrobial activity against *E. coli*, *Heliyon*, 5 (6), 01872.
- Fu, S., Thacker, A., Sperger, D. M., Boni, R. L. 2011, Relevance of Rheological Properties of Sodium Alginate in Solution to Calcium Alginate Gel Properties, *AAPS Pharm. Sci. Tech.*, 12 (2), 453-460.
- Gila Vilchez, C., Bonhome-Espinosa, A., Kuzhir, P., Zubarev, A., Duran, J. 2018, Rheology of magnetic alginate hydrogels, *Journal of Rheology*, American Institute of Physics, 62 (5), 1083-1096.
- Gombotz, W. R. 1998, Protein release from alginate matrices, *Advanced Drug Delivery Reviews*, 31 (3), 267-285.
- Grant, G. T., Morris, E. R., Rees, D. A., Smith, P. J. C., Thomas D. 1973, Biological interactions between polysaccharides and divalent cations: The egg-box model, *FEBS Lett.*, 32, 195-198.
- Hartati, Prasetyoko, D., Santoso, M., Qoniah, I., Leaw, W. I., Firda, P. B. D., & Nur, H., 2020, A review on synthesis of kaolin-based zeolite and the effect of impurities, *Journal of Chinese Chemical Society*, 67, 911-936.
- Hajifathaliha, F., Mahboubi, A., Nematollahi, S., Mohit, E., Bolourchian, N. 2020, Comparison of different cationic polymers efficacy in fabrication of alginate multilayer microcapsules, *Asian Journal of Pharmaceutical Sciences*, 15, 95-103.
- Kim, M. H., Lee, Y. W., Jung, W. K., Oh, J. & Nam, S. Y. (2019). Enhanced rheological behaviors of alginate hydrogels with carrageenan for extrusion-based bioprinting. *Journal of the Mechanical Behavior of Biomedical Materials*, 98(June), 187–194. <https://doi.org/10.1016/j.jmbbm.2019.06.014>
- Larsen, B. E., Bjørnstad, J., Petersen, E. O., Tønnesen, H. H., Melvik, J. E. 2015, Rheological characterization of an injectable alginate gel system., *Biotechnol.*, 15: 29, doi: 10.1186/s12896-015-0147-7.
- Liang, X., Ma, C., Yan, X., Zeng, H., McClements, D. J., Liu, X., & Liu, F. (2020). Structure, rheology and functionality of whey protein emulsion gels: Effects of double cross-linking with transglutaminase and calcium ions. *Food Hydrocolloids*, 102(June 2019), 105569. <https://doi.org/10.1016/j.foodhyd.2019.105569>
- Liu, S., Li, H., Tang, B., Bi, S., Li, L. 2016, Scaling law and microstructure of alginate hydrogel, *Carbohydrate Polymers*, 135, 101–109.
- Lee, B-B., Ravindra, P., Chan, E-S. 2013, Size and Shape of Calcium Alginate Beads Produced by Extrusion Dripping, *Chemical Engineering & Technology*, 36(10), 1627-1642.
- Ozu, M., Galizia, L., Acuña, C., Amodeo, G. 2018, Aquaporins: More Than Functional Monomers in a Tetrameric Arrangement, *Cells*, 7, 209-233.
- Ozu, M., Alvarez, H. A., McCarthy, A. N., Grigera, J. R., Chara, O. 2013, Molecular dynamics of water in the neighborhood of aquaporins, *Eur Biophys J.*, 42, 223–239.

- Perullini, M., Orias, F., Durrieu, C., Jobbágy, M., Bilmes, S.A. 2014, Co-encapsulation of *Daphnia magna* and microalgae in silica matrices, a stepping stone toward a portable microcosm, *Biotechnology Reports*, 4, 147-150.
- Sandolo, C., Matricardi, P., Alhaique, F., & Coviello, T. (2009). Effect of temperature and cross-linking density on rheology of chemical cross-linked guar gum at the gel point. *Food Hydrocolloids*, 23(1), 210–220. <https://doi.org/10.1016/j.foodhyd.2008.01.001>
- Schuster, E., Cucheval, A., Lundin, L. & Williams, M.A.K., 2011, Using SAXS to reveal the degree of bundling in the polysaccharide junction zones of microrheologically distinct pectin gels, *Biomacromolecules*, 12, 2583-2590.
- Sonego, J. M., Santagapita, P. R., Perullini, M., Jobbágy, M. 2016, Ca(II) and Ce(III) homogeneous alginate hydrogels from parent alginic acid precursor: a structural study, *Dalton Trans.*, 45 (24), 10050-10057.
- Spedalieri, C., Sicard, C., Perullini, M., Brayner, R., Coradin, T., Livage, J. Bilmes, S. A., Jobbágy, M. 2015, Silica@ proton-alginate microreactors: A versatile platform for cell encapsulation, *J. Mater. Chem. B*, 3 (16), 3189-3194.
- Sutka, M. R., Amodeo, G., Ozu, M. 2017, Plant and animal aquaporins crosstalk: what can be revealed from distinct perspectives, *Biophysical Reviews*, 10, 545-562.
- Traffano-Schiffo, M.V., Castro-Giraldez, M., Fito, P.J., Perullini, M., Santagapita, P.R. 2018, Gums induced microstructure stability in Ca(II)-alginate beads containing lactase analyzed by SAXS, *Carbohydrate Polymers*, 179, 402-407.
- Wang, B., Gao, B., Zimmerman, A. R., Zheng, Y., Lyu, H. 2018, Novel Biochar-Impregnated Calcium Alginate Beads with Improved Water Holding and Nutrient Retention Properties, *Biotechnology Reports*, 4, 147-150.
- Zazzali, I., Calvo, TRA, Ruíz-Henestrosa, VMP, Santagapita, PR, Perullini, M. 2019, Effects of pH, extrusion tip size and storage protocol on the structural properties of Ca (II)-alginate beads, *Carbohydrate polymers*, 206, 744-756.

Declaration of interests

☒ The authors declare that they have no known competing financial interests or personal relationships that could have appeared to influence the work reported in this paper.

☐ The authors declare the following financial interests/personal relationships which may be considered as potential competing interests:


Dr. Mercedes Perullini

02/26/2021

Highlights

- ✓ Ca-alginate beads provide eco-friendly alternatives for R&D+i
- ✓ Our low-cost automated system allows *in situ* evaluation of bead formation kinetics
- ✓ Gel front evolution and total volume change allow tracking mechanical behaviors
- ✓ Ultrastructural analyses confirm the viability of the proposed methodology
- ✓ The proposed method is versatile, practical and easy to implement for screening